Mitnik L.M., 2013, trang 63-72
Kỷ yếu Hội nghị Quốc tế "Biển Đông 2012", Nha Trang, 12-14/9/2012

# DYNAMIC OCEANIC AND ATMOSPHERIC PHENOMENA IN THE VIETNAMESE WATERS VIEWED BY SATELLITE MICROWAVE RADIOMETERS AND SARS

**Leonid M. Mitnik**
V.I. Il'ichev Pacific Oceanological Institute, FEB RAS, Russia
E-mail: mitnik@poi.dvo.ru

**Abstract:** A combined use of multi-sensor remote sensing and *in-situ* data for the analysis and interpretation of the dynamic oceanic and atmospheric phenomena in the coastal Vietnamese zone and in the open South-China Sea is considered. The dataset consists of ERS-1/2 SAR, Envisat ASAR and ALOS PALSAR precision and quick look images acquired in 1996-2012, Terra and Aqua MODIS images, scatterometer-derived winds, ADEOS-II AMSR and Aqua AMSR-E microwave measurements and other supplementary information. The oceanic phenomena, which were revealed on SAR images include the coastal and river fronts, upwellings, eddies, internal waves, natural and anthropogenic films, swells, etc. Mesoscale spiral eddies the size of 5-10 km were detected due to filamentary slicks mainly in the coastal zone. Surface expressions of oceanic internal waves were observed both in the coastal zone and in the open sea. Integrated atmospheric parameters and sea surface wind speed have been estimated in tropical cyclones, fronts and other marine weather systems from the Advanced Microwave Scanning Radiometer for the Earth Observing System (AMSR-E) of Aqua, from the QuikSCAT and ASCAT scatterometers.

**Key words:** *SAR, Microwave radiometers, Coastal fronts, Eddies, Internal Waves, River plumes, Oil spills, Tropical cyclones, Wind speed.*

## I. INTRODUCTION

The *oceanic dynamic features* (*current fronts, eddies, upwellings, internal waves, river plumes*, etc.) as well as the imprints of the *atmospheric phenomena* of various scales (*tropical cyclones, mesoscale convective rolls and cells, squall lines, rain cells*, etc.) were revealed by analysis of high-resolution Synthetic Aperture Radar (SAR) images of the Vietnam Sea acquired in 1991-2012 from the ERS-1/2, Envisat and ALOS satellites for several POI projects with the European Space Agency (ESA) and the Japan Aerospace Exploration Agency (JAXA). A spaceborne SARs provide unique near-all-weather high-resolution views of the sea surface. These finely detailed images constitute some of the most complex and least understood data provided by remote sensing. The sea surface can contain the signatures of such diverse phenomena as current boundaries, eddies, upwelling, surface and internal waves, shallow water bathymetry, surface films and objects, wind, storms, rainfall, convective rolls and cells. They manifest themselves on the images as brightness variations that in turn are due to the changes of the sea surface roughness field. The interpretation of SAR signatures can be vastly improved by the concurrent analysis of data collected by visible, infrared and

microwave sensors (Jackson, Apel, 2004; Mitnik, Dubina, 2010; Robinson, 2010). Temporal coverage of satellite SARs is, however, low.

Quantitative characteristics of the *marine weather systems* (water vapor content, cloud liquid water and sea surface wind speed) were obtained by processing of Aqua AMSR-E microwave radiometer measurements with the usage of original retrieval algorithms (Mitnik, Mitnik, 2003; 2006; 2011). Ancillary data consisted of the Terra and Aqua MODIS images, QuikSCAT and ASCAT scatterometer-derived wind fields, surface analysis maps, etc.

High probability of cloudiness over the Vietnamese waters enhances necessity to use passive and active microwave sensors for detailed monitoring of the dynamic phenomena in the ocean-atmosphere system. Regular passive microwave sensing from several satellites including recently launched American NOAA-19, DMSP F-18 and Suomi NPP, Indian Megha-Tropiques, Japanese GCOM-W1, Chinese Fengyun-3, etc. improved significantly the temporal resolution that is vital to generate nowcasts and short-time weather forecasts and to decrease losses caused by storm winds, precipitation and floodings. The spatial resolution of passive microwave data is, however, significantly worse compare to SAR images and as a result many important medium-scale and fine-scale details of the oceanic dynamic phenomena are smoothed or disappear.

The waters surrounding Vietnam, especially its coastal zone, are characterized by very high physical and biological variability in both time and space. The approach based on utilization of passive and active microwave sensors separately and in combination was investigated to take advantage of each instrument's unique monitoring capabilities. The AMSR-E provided (till October 2011) and GCOM-W1 provides (since July 2012) 2-3 daily coverage of synoptic-scale and mesoscale atmospheric phenomena, allowing the estimation of the total water vapor content *V*, total cloud liquid water content *Q*, precipitation *R*, sea surface wind speed *W* and Sea Surface Temperature (SST). Below several examples of satellite passive and active microwave data acquired over the Vietnamese waters are considered and interpreted.

## II. MATERIALS AND METHODS

### 1. Synthetic Aperture Radar images (1992-2012)

The main characteristics of satellite SARs are given in Tab. 1.

**Table 1.** Characteristics of satellite Synthetic Aperture Radars

| Satellite | ERS-1/2 | Envisat | ALOS |
|---|---|---|---|
| Sensor | SAR | SAR | PALSAR |
| Frequency, GHz | 5.3 | 5.3 | 1.27 |
| Wavelength, cm | 5.6 | 5.6 | 23.6 |
| Polarization | VV | VV, HH | VV, HH, VH, HV |
| Incidence angle, deg | 20-26 | 15-45 (variable) | 8-60 (variable) |
| Swath width, km | 100 | 100-405 | 20-350 |
| Resolution, m | 25 x 25 | 25 x 25, 150x150 | 7 -100 |

### 2. Aqua AMSR-E brightness temperatures (2003-2011)

The main characteristics of AMSR-E radiometer are the following: frequencies 6.9, 10.7, 18.7, 23.4, 36.5 and 89.0 GHz, V- and H-polarizations, incidence angle ≈55º, conical scanning, swath width 1450 km, instant field of view 35x62 km at 6.9 GHz 24x41 km at 10.7 GHz, 14x22 km at 18.7 GHz, 15x26 km at 23.6 GHz, 7x12 km at 36.5 GHz, and 3x5 km at 89.0 GHz. Sampling interval is 5x5 km at 89.0 GHz and 10x10 km at all other frequency channels (Kawanishi et al., 2003).

### 3. Ancillary data

- Terra and Aqua MODIS visible and infrared images (2003-2012)
- QuikSCAT (2003-2009) and MetOp ASCAT (2006-2012)–derived wind fields.

## III. RESULTS

### 1. Oceanic dynamic phenomena

*1.1.* Fig. 1 shows coastal fronts revealed on Envisat ASAR images acquired in October 2011.The fronts manifest themselves as narrow elongated contrast lines. Increased brightness of these signatures is due to the increased sea surface roughness caused by wave breaking in the narrow frontal zones where current shift is observed.

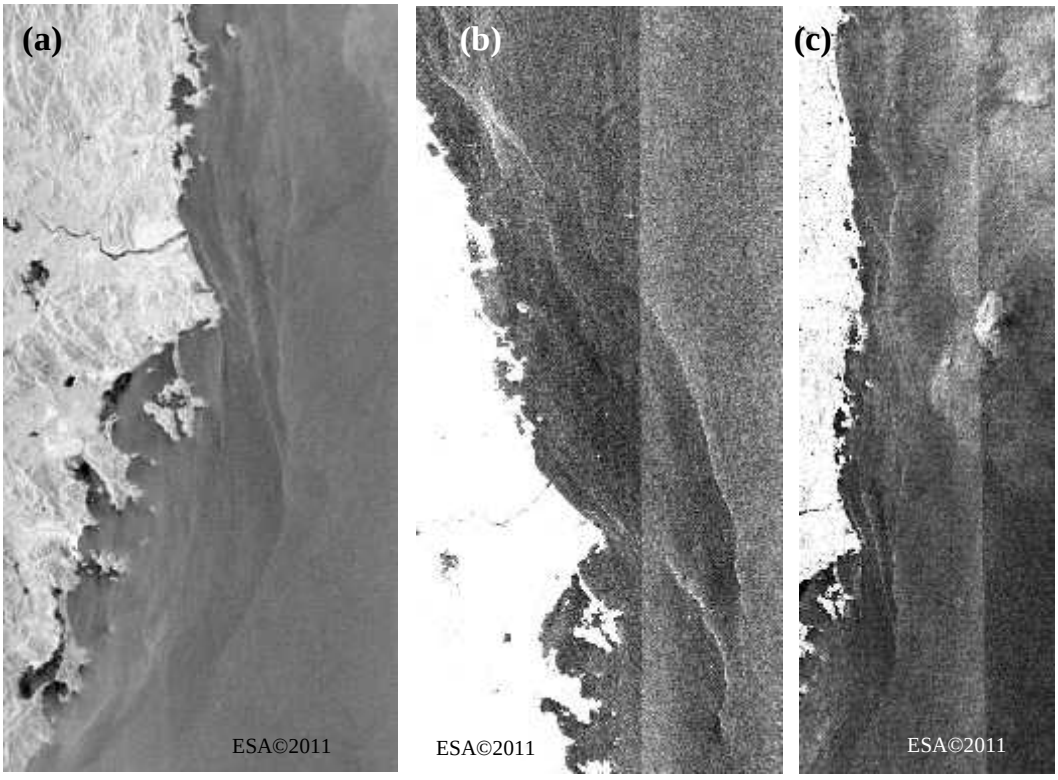


**Figure 1.** Coastal fronts on Envisat ASAR images acquired on 19 October (a), 25 October (b) and 31 October (c) 2011.

*1.2.* The similar features were detected in the areas of river plume where the sharp boundaries divide the water masses possessing by different physical, chemical and biological properties. The location and appearance of these frontal signatures is determined by bottom topography, river discharge and environmental conditions. Likely, the area and shape of river plumes can be used as integrated parameters associated with fresh water discharge through individual river cut-offs depending on precipitation variations over a particular watershed. (Mekong River plume on ERS-1 image can be found at web site: The tropical and subtropical ocean viewed by ERS SAR (http: //earth.esa.int/ers/instruments/sar/applications/ERS-SARtropical/). The Mekong River plume features were regularly detected on images taken both C-band and L-band satellite SARs (Fig. 2). The appearance of the bright frontal signatures on both images allows concluding that there is modulation of centimeter- and decimeter-wavelength wind waves responsible for backscattering of C- and L-band SAR signals, correspondingly.

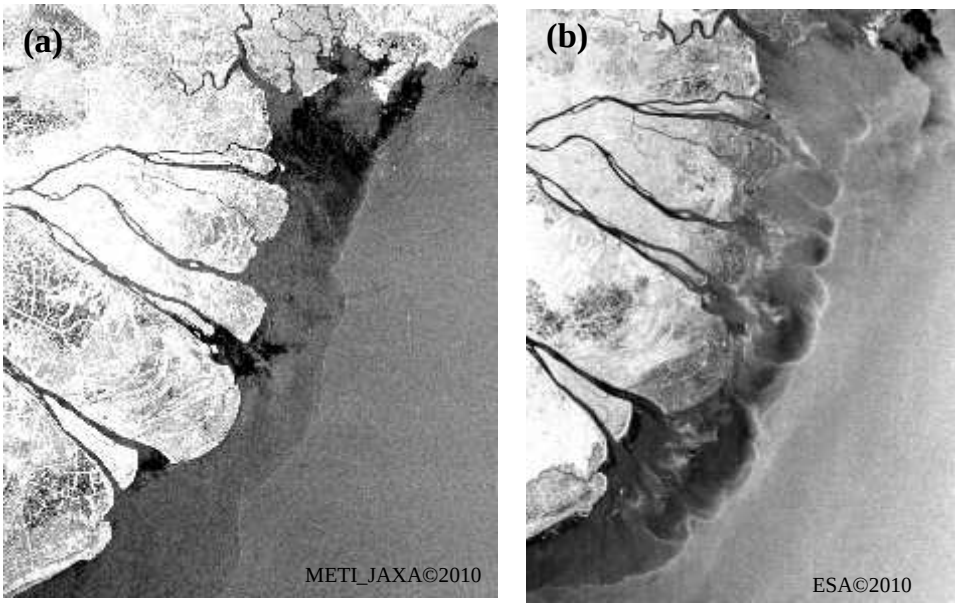


**Figure 2.** Mekong River plume observed by L-band PALSAR on 18 November 2010 (a) and C-band ASAR on 3 January 2011 (b). ALOS METI and JAXA.

*1.3.* Eddy structures of various scales and shape were observed in the coastal zone and in the open sea (Ivanov, Ginzburg, 2002; Johannessen et al., 2006; Robinson, 2010). Eddies’ visibility on SAR images was due to current-waves interaction (dynamic factor) and/or due to the increased concentration of surface films. Fig. 3 depicts Envisat ASAR image acquired on 25 October 2011 and an enlarged fragment showing detailed structure of cold eddy 1 the size of approximately 170 km. The circular wave features within the eddy result from cyclonic movement of surface water. The wavelength of these waves varies from 700 till 1200 m. In situ current and hydrographic measurements during the early September cruise and concurrent satellite altimeter observations in this area allowed constructing three-dimensial structure of cold eddy (Hu et al., 2011). Bright dots within the eddy are ships. Digits 2 and 3 on the image mark linear features (coastal fronts) and chains of circular features (rain cells) (Fig.3a).

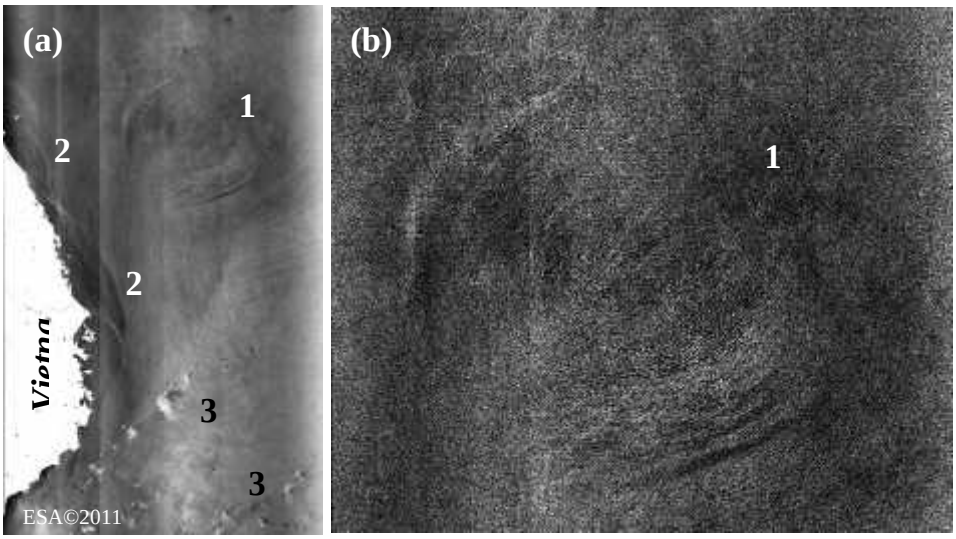


**Figure 3.** Envisat ASAR image of the Vietnamese waters acquired on 25 October 2011 (a) and an enlarged fragment showing circular features within cold eddy (b)

*1.4.* Surface manifestations of the internal waves (IWs) are the typical well-defined signatures of the SAR images. IWs were observed both in the coastal zone and in the open sea. These signatures are used to determine the probable regions of their generation and estimate a number of parameters such as wavelengths, propagation velocity, etc. (Jackson, Apel, 2004; Robinson, 2010). Two images in Fig. 4 show several packets of IWs in the coastal Vietnam zone.

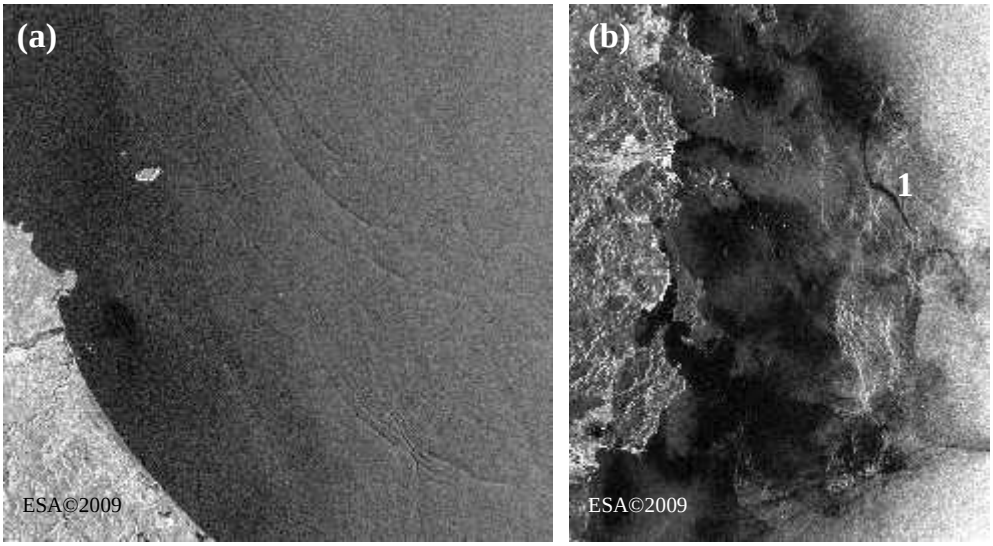


**Figure 4.** Internal waves near Vietnam coast on Envisat ASAR images acquired on 1 July at 02:34 UTC (a) and on 24 August at 02:38 UTC (b) 2009. 1 – oil spill.

*1.5.* Kilometer-scale eddies and filamentary natural films were found on many Envisat ASAR images (Fig. 5). They were detected as the darker features against the background due to damping of the small-scale sea surface roughness by natural films. Dark lines, bands and patches were also caused by oil spills associated with fishery, shipping and river freshwater drainage. Oil films can be

observed at higher wind speed compare to biological ones. The last one covering the sea east of Nha-Trang was acquired on 21 February 2012 at 21:37 UTC. Detection and interpretation of the dark signatures on ERS-1/2, Envisat and ALOS SAR images and also description of oil behavior at the sea, techniques, references, links, etc. are considered in web site: http://cearac.poi.dvo.ru). Database consists of 120 cases; annotation is given for 47 SAR images.

**Figure 5.** Envisat ASAR image of the open South-China Sea acquired on 13 March 2010 at 02:19 UTC showing spiral eddy 1, oil spill 2, arciform imprints of internal waves at the upper right, numerous filamentary slicks and ships (bright dots).

## 2. Atmospheric phenomena

*2.1.* Storm wind and precipitation are the main atmospheric factors hindering marine fishery and shipping in the Vietnamese waters and farmwork in Vietnam. Quantitative characteristics of the marine weather systems can be derived from satellite observations almost in real time. Consider satellite observations of tropical cyclone Nesat. It made landfall over the northeastern part of Hainan Island in the afternoon on 29 September. On 30 September, Nesat first weakened into a severe tropical storm and moved across Beibu Wan, then made landfall again over the coast of northern Vietnam in the afternoon and weakened into a tropical storm. It moved further inland that evening and dissipated over northern Vietnam on 1 October. In Vietnam around 3000 houses were destroyed and 11 boats sank during the passage of Nesat.

Satellite observations of Nesat acquired on 30 September are presented in Fig. 6. Brightness of ASAR image increases with the increase of wind speed. The

cyclone center 1 is clearly seen as a dark circular area surrounding by storm wind area 2. Bands of the alternating brightness 3 are caused by coastal orography: wind speed decreases downstream of mountains (wind shadows). Weak winds were observed near the coast (dark areas 4). Wind field derived from MetOp ASCAT sensing indicates the same features as in ASAR image (Fig. 6b).

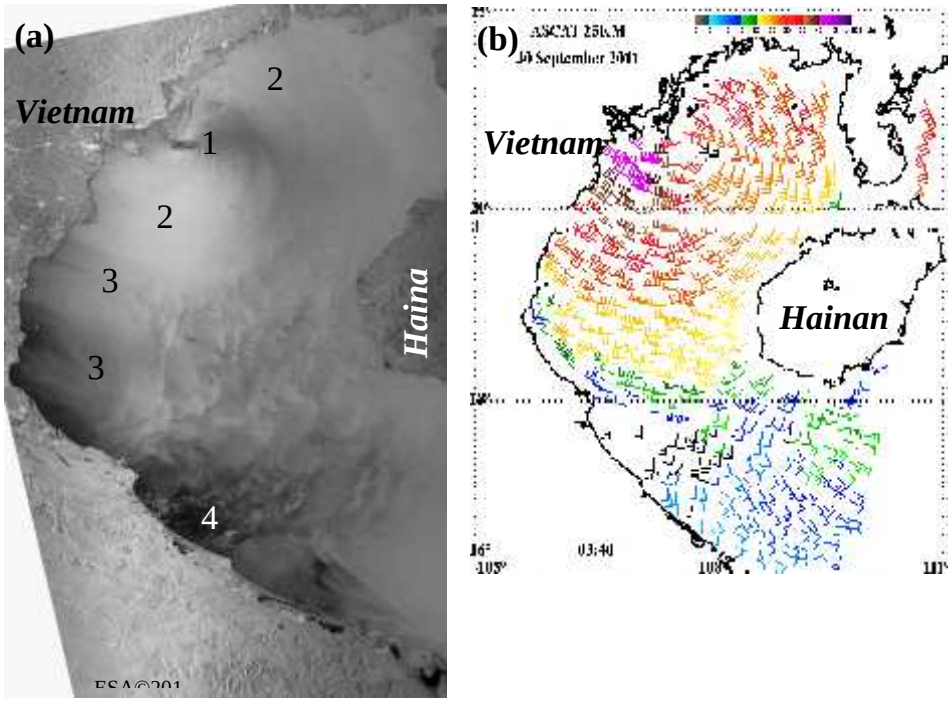


**Figure 6.** Satellite observations of cyclone Nesat during its landfall on 30 September 2011: Envisat ASAR image taken at 02:51 UTC (a) and MetOp ASCAT-derived wind field at 03:40 UTC (b).

*2.2.* Satellite passive microwave sensors provide fields of the brightness temperatures $T_B^{v,h}(\nu)$ at several frequencies ν with vertical (v) and horizontal (h) polarizations used for retrieval of sea surface temperature, sea surface wind speed, total atmopsheric water vapor content, total cloud liquid water content, precipitation (Gentemann et al., 2010; Mitnik, Mitnik, 2003, 2010; Mitnik et al., 2007). Evolution of tropical cyclones over the South-China Sea was studied with $T_B^{v,h}(\nu)$ measured by Aqua AMSR-E radiometer together with data provided by TRMM TMI, Terra and Aqua MODIS, QuikSCAT and ASCAT scatterometers.
An example of microwave data processing over typhoon Megi is shown in Fig. 7. Typhoon structure manifests itself in cloud field: low values of cloud liquid water content $Q$ in the eye surrounding by eye wall where $Q > 2$ kg/m$^2$, spiral rain bands which are also characterized by high $Q$-values and large area with $Q = 0.8 – 1.2$ kg/m$^2$ (Fig. 7a). Heavy clouds and rains hinder wind speed estimate. The corresponding area is marked by white color in Fig. 7a. Within this zone wind speed can reach the highest values that confirm scatterometer data in Fig. 7c. However direct comparison of wind fields retrieved by passive and active sensors is not so straightforward due to different mechanisms resposible for formation of

the increased sea surface emissivity and surface waves backscattering, differences in spatial resolution, and other factors.

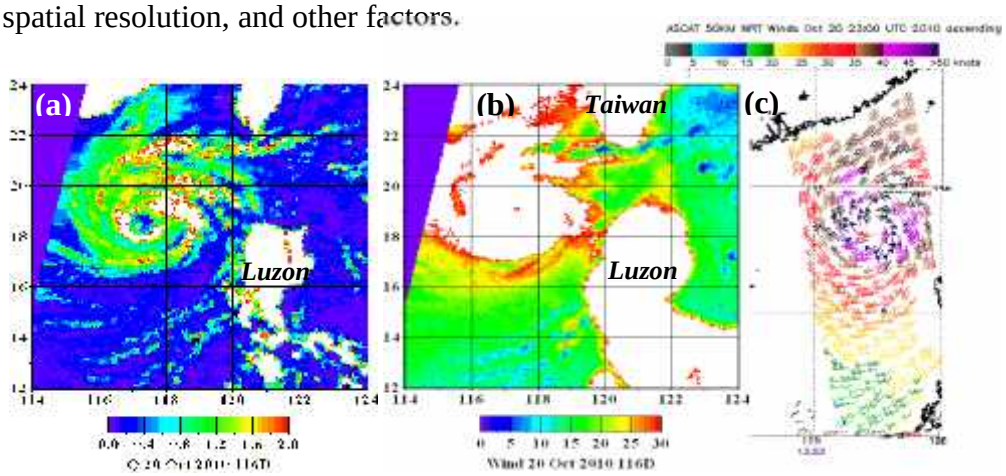


**Figure 7.** Total cloud liquid water content in kg/m$^2$ (a) and wind speed in m/s (b) retrieved from Aqua AMSR-E at 17:38 UTC and MetOp ASCAT wind speed (in knots) at 13:53 UTC (c) on 20 October 2010

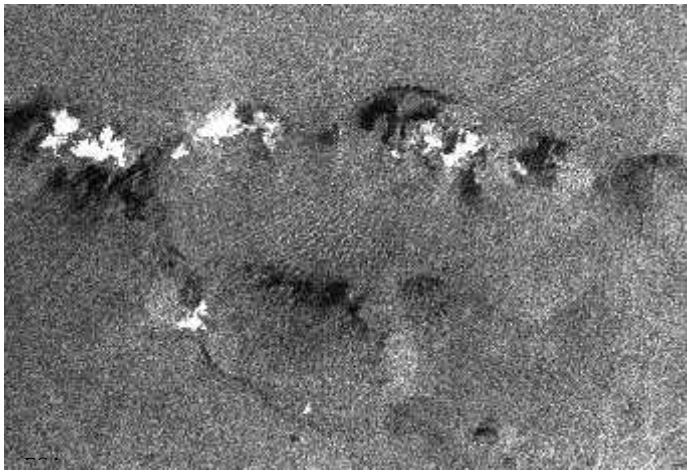

**Figure 8.** Fragment of Envisat ASAR image the size of approximately 80 x 60 km acquired on 17 September 2011 at 02;28 UTC showing chain of rain cells as bright and dark patches against the gray-tone waters.

Individual rain cells are smoothed by large field of view of satellite microwave radiometers. They, however, can be distinguished on SAR images due to their impact on the sea surface. This impact results from modulation of the sea surface roughness by falling rain drops and squall lines that are observed at the cells boundaries (Atlas, 1994; Jackson, Apel, 2004). Rain signatures are very variable and appear darker and brighter patches against the surrounding waters, which have a grey tone on the image. Narrow strait and curved light lines are surface manifestations of several packets of internal waves

## IV. DISCUSSIONS

Satellite data collected by sensors operating in microwave, infrared and visible spectral bands and obtained over the same scenes demostrate the high potential of

their joint analysis. It follows from differences in atmospheric attenuation and in spatial resolution as well as in mechanisms of formation of the brightness contrasts at different wavelengthes. Experimental data should be compared with the results of model calculations carried out with the upgradet models of rasdiative transfer in the ocean-atmopshere system that, in particular, can serve as the basis for development of algorithms of geophysical retrievals (Gentemann et al., 2010; Mitnik et al., 2007). This approach was used to study the oceanic and atmopsheric phenomena in the Vietnamese waters including typhoons. Wind, waves and heavy rains accompanying tropical cyclones affect near shore hydro- and morphodynamics and are perhaps the most important factor shaping coastal evolution in Vietnam especially near large river mouths and deltas (Ostrowski et al., 2009). Continuation of time series of satellite data using, in particular, recently launched American Suomi NPP, Japanese GCOM-W1, Indian Megha-Tropiques and RISAT-1 and planned to launch European Sentinal-1 and Japanese ALOS-2 satellites will allow to trace the evolution of the oceanic and atmopsheric processes and detect their short-time, seasonal and interannual changes.

## V. CONLUSIONS

The ERS-1/2 SAR, Envisat ASAR and ALOS PALSAR images have demonstrated the new possibilities to study the highly variable dynamic phenomena in the Vietnamese surface waters such as current fronts, eddies of various scales, river plumes, internal waves, oil spills, etc as well as the atmospheric phenomena using their manifestations in the sea surface roughness field. Only several examples were considered.

The results of more comprehensive study of various oceanic and atmopsheric phenomena and processes with the usage of multisensor satellite and *in situ* data together with the surface current simulations will improve understanding of mechanisms responsible for generation and evolution of the revealed phenomena. The knowledge of these mechanisms is important both for solving oceanographic problems such as formation of high-productive fishery grounds and interaction riverine and marine waters and for development of SAR backscatter models. Important components of the input data in models are surface wind and precipitation which are also estimated from satellite remote sensing.

**Acknowledgement.** This work was supported by the Russian Fond for Basic Research Project 11-05-ophi-m-2011 and Federal Program "World Ocean". Author thanks the European Space Agency for providing ERS-1/2 and Envisat ASAR images and the Japan Aerospace Exploration Agency for providing Aqua AMSR-E and ALOS PALSAR data and Yu.A. Kuzlyakina for satellite image processing.

## REFERENCES

1. Atlas, D., 1994. Origin of storm footprints on the sea seen by synthetic aperture radar, *Science*, 266(5189): P. 1364–1366.
2. Gentemann, C.I., F.J. Wentz, M. Brewer, K. Hilborn, D. Smith, 2010. Passive microwave remote sensing of the Ocean: An overview. In: Ocean from Space.

Revisited. B. Vittorio, J.F.R. Gower, L. Alberotanza (eds.), Springer, 13-33 pp. DOI 10.1007/978-90-481-8681-5_2.
3. Jackson, C.R., J.R. Apel, 2004. Synthetic Aperture Radar Marine User's Manual / http://www.sarusersmanual.com/
4. Johannessen, J.A., L.H. Pettersson, T. Eldevik, D. Durand, G. Evensen, N. Winther, O. Breivik, 2006. Coastal physical and biochemical processes. In: Remote Sensing of the Marine Environment, J.F.R. Gower (ed.). American Society for Photogrammetry and Remote Sensing, Bethesda, Maryland, 179–196 pp.
5. Ivanov, A.Yu., A.I. Ginzburg, 2002. Oceanic eddies in synthetic aperture radar images, *Proc. Indian Academy of Sciences (Earth Planetary Sciences*). 111(3): 281-295.
6. Kawanishi T., Sezai. T., Y. Ito, K. Imaoka, T. Tukeshima, Y. Ishido, A. Shibata, M. Miura, H. Inahata, R.W. Spencer, 2003. The Advanced Microwave Scanning Radiometer for the Earth Observing System (AMSR-E). NASDA’s contribution to the EOS for global energy and water cycle studies, *IEEE Transactions Geoscience Remote Sensing.* 41 (2): 184-194.
7. Mitnik, L.M., V.A. Dubina, 2010. Interpretation of SAR signatures of the sea surface: A multi-sensor approach. In: Ocean from Space. Revisited. B. Vittorio, J.F.R. Gower, L. Alberotanza (eds.), Springer, 113-130 pp. DOI 10.1007/978-90-481-8681-5_7.
8. Mitnik, L.M., M.L. Mitnik, 2003. Retrieval of atmospheric and ocean surface parameters from ADEOS-II AMSR data: comparison of errors of global and regional algorithms, *Radio Science*. 38(40): 8065, doi: 10.1029/2002RS002659.
9. Mitnik, L.M., M.L. Mitnik, 2010. AMSR-E advanced wind speed retrieval algorithm and its application to marine weather systems. In: Proc. 2010 IEEE Intern. Geoscience and Remote Sensing Symposium, Hawaii, 26-30 July 2010. ISBN 978-1-4244-9566-5. P. 3224-3227.
10. Mitnik, L.M., M.L. Mitnik, V.A. Dubina, 2007. Remote radiophysical sensing of ocean-atmosphere system, In: FarEastern Russian Seas, V.A. Akulichev (ed) Moscow, Nauka, Book. 4. Physical Research Techniques. P. 449-537 (in Russian).
11. Ostrowsky, R., Z. Pruszak, G. Rózynski, M. Szmytkiewicz, Pham Van Ninh, Do Ngoc Quynh, Nguyen Thi Viet Lien, 2009. Coastal processes at selected shore segments of South Baltic Sea and Gulf of Tonkin (South China Sea), *Archives of Hydro-Engineering and Environmental Mechanics.* 56 (1–2). P. 3–28.
12. Robinson, I.S., 2010. Discovering the Ocean from Space: the Unique Applications of Satellite Oceanography, Berlin, Germany, Springer/Praxis Publishing, 638pp.